

SHORT-LIVED ²⁴⁴Pu POINTS TO COMPACT BINARY MERGERS AS SITES FOR HEAVY R-PROCESS NUCLEOSYNTHESIS

KENTA HOTOKEZAKA, TSVI PIRAN, AND MICHAEL PAUL
 Racah Institute of Physics, The Hebrew University, Jerusalem, 91904, Israel.
Draft version July 26, 2018

ABSTRACT

Measurements of the radioactive ²⁴⁴Pu abundances can break the degeneracy between high-rate/low-yield and low-rate/high-yield scenarios for the production of heavy *r*-process elements. The first corresponds to production by core collapse supernovae (cc-SNe) while the latter corresponds to production by e.g. compact binary mergers. The estimated ²⁴⁴Pu abundance in the current interstellar medium inferred from deep-sea measurements (Wallner et al. 2015) is significantly lower than that corresponding Early Solar System abundances (Turner et al. 2007). We estimate the expected median value of the ²⁴⁴Pu abundances and fluctuations around this value in both models. We show that while the current and Early Solar System abundances are naturally explained within the low-rate/high-yield (e.g. merger) scenario, they are incompatible with the high-rate/low-yield (cc-SNe) model. The inferred event rate remarkably agrees with compact binary merger rates estimated from Galactic neutron star binaries and from short gamma-ray bursts. Furthermore, the ejected mass of *r*-process elements per event agrees with both theoretical and observational macronova/kilonova estimates.

Subject headings:

1. INTRODUCTION

The origin of heavy *r*-process elements is one of the current nucleosynthesis mysteries (Cowan et al. 1991; Qian & Wasserburg 2007; Arnould et al. 2007). Core collapse supernovae (Burbidge et al. 1957) and compact binary mergers are considered as possible sites (Lattimer & Schramm 1974; Eichler et al. 1989; Freiburghaus et al. 1999). The first produces small amounts of material at a high event rate while the latter produces large amounts in rare events. Radioactive elements, with the right lifetime can break the degeneracy between high-rate/low-yield and low-rate/high-yield scenarios. Among radioactive elements most interesting is ²⁴⁴Pu (half-life of 81 Million years) for which both the current accumulation of live ²⁴⁴Pu particles accreted via interstellar particles in the Earth's deep sea floor (Wallner et al. 2015) and the Early Solar System (ESS) abundances have been measured (Turner et al. 2007). Interestingly, the estimated ²⁴⁴Pu abundance in the current interstellar medium (ISM) inferred from deep-sea measurements is significantly lower than that corresponding to the ESS measurements.

Using a model for the mixing of the heavy elements within the Galaxy we calculate the estimated median abundance and the fluctuation around this value in both scenarios and compare the results with astronomical observations.

2. TOTAL HEAVY R-PROCESS PRODUCTION

Using the Solar abundance (Goriely 1999) as the mean value for stars in the Galactic disk, the total mass of heavy *r*-process elements ($A \geq 90$) in the Galaxy is $M_{\text{tot}, A \geq 90} \approx 5 \times 10^3 M_{\odot}$. These elements show a uniform abundance pattern in metal-poor stars (Snedden et al. 2008), suggesting that they are produced in a single kind

of event. The total mass yields a relation between the Galactic event rate, R , and the heavy *r*-process mass produced in each event $M_{\text{ej}, A \geq 90}$ (see Fig. 1):

$$\langle R \rangle \approx 50 \text{ Myr}^{-1} \left(\frac{M_{\text{ej}, A \geq 90}}{0.01 M_{\odot}} \right)^{-1}. \quad (1)$$

Here $\langle R \rangle$ is the rate averaged over the age of the Galaxy and it is not necessarily the same as the present-day event rate R_0 . For sources related to the death of massive stars the event rate should follow the star formation rate which at present is lower than the average value (Hopkins & Beacom 2006). For compact binary mergers, the event rate follows with some delay the star formation rate. The event rate of short gamma-ray bursts (SGRBs; Wanderman & Piran 2015) that likely arise from compact binary mergers (Eichler et al. 1989), increases with the cosmological redshift z at least up to $z \approx 0.8$. In both cases, R_0 may be smaller than $\langle R \rangle$ by up to a factor of ~ 5 .

3. MEASURED SHORT LIVED ²⁴⁴Pu ABUNDANCES

Using the total mass alone we cannot distinguish between the high-rate/low-yield and the low-rate/high-yield sources. Measurements of abundances of short-lived radioactive *r*-process nuclides can, however, remove this degeneracy, as these abundances reflect the *r*-process production history on timescales comparable to their lifetimes (modulo the Galactic mixing timescale). Among the various radioactive nuclides, ²⁴⁴Pu seems most suitable: (i) it is produced only via the *r*-process; (ii) the half-life of ²⁴⁴Pu, 81 Million years (Myr), is sufficiently short compared to the Hubble time, while long enough to allow for significant accumulation; (iii) both current and ESS (~ 4.6 Gyr before present; BP) ²⁴⁴Pu abundance in the ISM have been measured.

The inner Solar System continuously accretes interstellar dust grains (Mann 2010) containing recently pro-

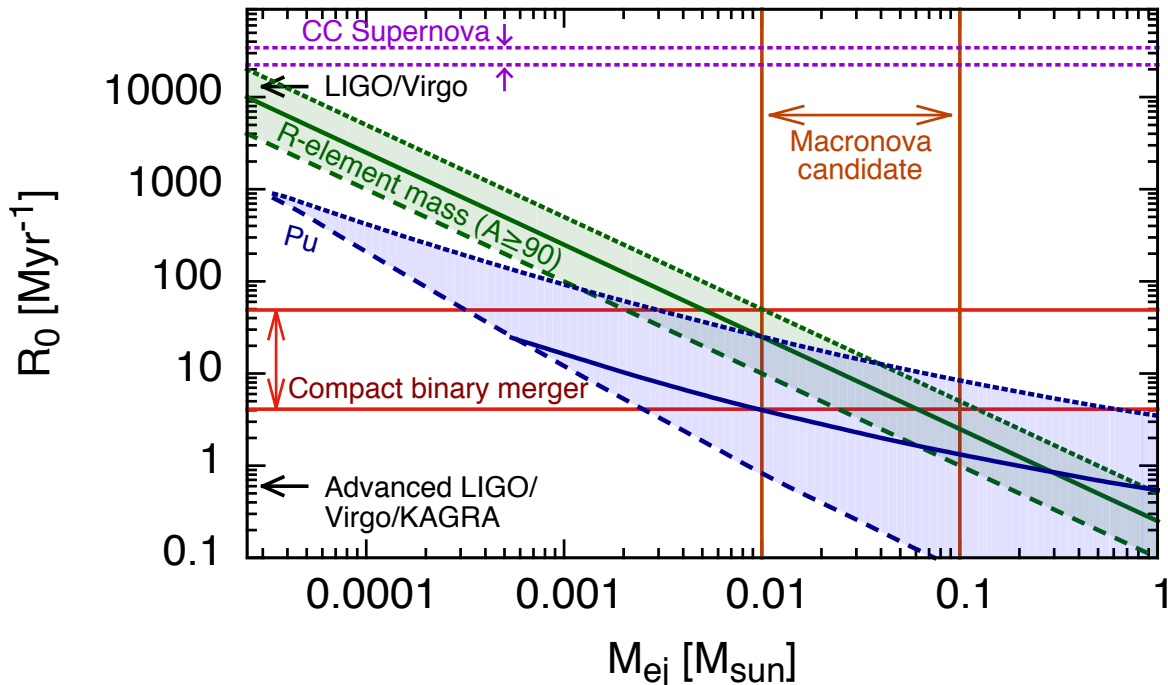


FIG. 1.— The heavy r -process event rate and the ejected mass. The diagonal green region expresses the degeneracy between high-rate/low-yield and low-rate/high-yield corresponding to the total mass of (stable) r -process elements in the Galaxy, with $R_0 = \langle R \rangle$, $0.5\langle R \rangle$, and $0.2\langle R \rangle$ (see Eq. 1). The allowed region inferred from the ^{244}Pu abundance in the deep-sea crust (Wallner et al. 2015) and the ESS (Turner et al. 2007; Lodders et al. 2009) is shown as a blue band. The blue solid (dotted) line corresponds to the current ISM ^{244}Pu density being the median (2σ) value. The region above the dashed blue line is the allowed region consistent with the ESS measurement (within 2σ fluctuations and taking into account that the rate at 4.6 Gyr BP can be higher than R_0 by up to a factor of 5). The current event rate estimated from binary neutron stars (Kim et al. 2015) and SGRBs (Wanderman & Piran 2015) are shown as the region between the horizontal red lines. For SGRBs, we take an unknown jet beaming factor in the range 10 – 70. The region between the horizontal dotted purple lines corresponds to the cc-SNe event rate (Li et al. 2011). Macronova mass estimates (Rosswog 2013; Hotokezaka et al. 2013; Bauswein et al. 2013; Tanvir et al. 2013; Berger et al. 2013; Yang et al. 2015) are between the vertical dark orange lines. The upper and lower horizontal arrows show the LIGO/Virgo upper limit of the merger (Abadie et al. 2012) and the expected capability of the advanced gravitational-wave detectors with 5 yr observations. The overlap region of the ^{244}Pu measurements and the total amount of heavy r -process element s is consistent with that of the compact binary merger scenario.

duced live radioactive ^{244}Pu . (Wallner et al. 2015) (see also Paul et al. 2001) measured the accumulation of ^{244}Pu in a deep-sea crust sample during the last 25 Myr and estimated the ^{244}Pu flux on the Earth’s orbit as $250_{-205}^{+590} \text{ cm}^{-2} \text{ Myr}^{-1}$, where the upper and lower values correspond to 2σ limits¹. The corresponding mean number density of ^{244}Pu in the ISM is $6 \times 10^{-17} \text{ cm}^{-3}$ and the 2σ upper limit is $2 \times 10^{-16} \text{ cm}^{-3}$ (see Appendix). These values are significantly lower than the number density in the ISM determined from the ESS ^{244}Pu abundance: $n_{\text{Pu}} \approx (^{244}\text{Pu}/^{238}\text{U})_{\text{ESS}} Y_{\text{U,ESS}} n_{\text{ISM}} \sim 6 \times 10^{-15} \text{ cm}^{-3}$. The relative abundance ratio of $(^{244}\text{Pu}/^{238}\text{U})_{\text{ESS}} \approx 0.008$ is estimated from fissionogenic xenon in ESS material (Turner et al. 2007). $Y_{\text{U,ESS}} = 7.3 \times 10^{-13}$ is the number abundance of ^{238}U relative to hydrogen inferred from meteorites (Lodders et al. 2009; corrected from the present for ^{238}U decay) and n_{ISM} is the mean number

¹ Wallner et al. (2015) analyze two samples, crust and sediment. Here we focus on the crust sample that statistically dominates over the sediment one and spans a longer accumulation time (see Appendix).

density of the ISM, which is typically $\approx 1 \text{ cm}^{-3}$.

4. CHEMICAL MIXING PROCESSES AND MEDIAN ^{244}Pu ABUNDANCE

The abundance of a radioactive nuclide at a given location around the solar circle, r_{\odot} , depends on the event rate density, $\mathcal{R} \equiv \rho_*(r_{\odot}, 0)R/M_* \approx 0.0015R \text{ Myr}^{-1} \text{ kpc}^{-3}$, where $\rho_*(r, z)$ is the stellar mass density in the disk, r and z are the Galactic radius and height above the Galactic plane, and M_* is the total stellar mass in the disk (McMillan 2011).

The abundance depends also on the mixing timescale. Heavy nuclei ejected into the ISM are homogenized via different processes on different timescales (Roy & Kunth 1995). Initially, the gas containing heavy nuclei expands into the ISM as a blast wave until after a couple of Myr (Cioffi et al. 1988), depending on the ejecta’s kinetic energy, initial velocity and external density. In the literature, it has been often assumed that at this stage the ejected material remains within this fluid element, yielding a very slow process of mixing within the galaxy. However, the ISM turbulence efficiently homog-

enizes the ejected material (Scalo & Elmegreen 2004). The diffusion timescale of the nuclei is determined by the turnover timescale of the largest eddies (Pan & Scannapieco 2010). The diffusion coefficient can be described as $D \equiv v_t l_{\text{mix}}/3 \simeq \alpha \text{ kpc}^2/\text{Gyr}$ ($v_t/7 \text{ km s}^{-1})(H/0.2 \text{ kpc})$, where v_t is the typical turbulent velocity of the ISM, $l_{\text{mix}} = 3\alpha H$ is the turbulence mixing length and H is the scale-height of the local ISM. Here we have introduced a mixing length parameter α , choosing $\alpha = 0.1$ as a reference value. A numerical simulation of the turbulent mixing in the Galactic disk shows this level of efficiency of the mixing (Yang & Krumholz 2012). Defining τ_{mix} as the mean time between injection events at a given location, $(4\pi R\tau_{\text{mix}}/3)^{-1/3} \equiv 2(D\tau_{\text{mix}})^{1/2}$, we have:

$$\tau_{\text{mix}} \approx 300 \text{ Myr} (R/10 \text{ Myr})^{-2/5} (\alpha/0.1)^{-3/5} (v_t/7 \text{ km/s})^{-3/5} (H/0.2 \text{ kpc})^{-3/5}. \quad (2)$$

The median number density² of a short-lived radioactive nuclide with a mean-life τ_i is:

$$\langle n_i \rangle_m \approx n_{\text{eq},i} \exp\left(-\frac{\tau_{\text{mix}}}{2\tau_i}\right), \quad (3)$$

where $n_{\text{eq},i} \approx N_i \mathcal{R} \tau_i$ is the equilibrium value and N_i is the total number of the nuclide i ejected by each event.

For $\tau_i \gg \tau_{\text{mix}}$, a typical observer measures $n_{\text{eq},i}$. For $\tau_i \ll \tau_{\text{mix}}$, a typical observer measures a number density much lower than $n_{\text{eq},i}$ and one needs a larger yield to reach an observed value, interpreted here as the median number density. Figure 1 depicts the needed rate and yield so that the current ^{244}Pu is the median value for typical values of α , v_t and H (see Eq. 2). This relation (blue area in Fig. 1) becomes flatter than $R \propto M_{\text{ej}}^{-1}$ (Eq. 1, green band in Fig. 1) for decreasing event rates breaking the rate-yield degeneracy.

5. MONTE-CARLO SIMULATION OF ^{244}Pu ABUNDANCE

In order to take into account the large fluctuation in the measured number density averaged over timescales shorter than τ_{mix} , we simulate the history of the ^{244}Pu abundance in the ISM around the solar circle over the last 7 Gyr. We take into account the radioactive decay, the turbulent diffusion process and the time evolution of the production rate. The r -process events are generated randomly in a 4-dimensional box with dimensions 7 Gyr in time, $16.66\pi \text{ kpc}$ in the x -direction (the circumference of the solar circle), 2 kpc in the y -direction (the width of the circle), and an exponential decay in the z -direction (the height from the Galactic plane). The events are distributed following the stellar mass distribution in the Galactic disk McMillan (2011) and the redshift evolution following the SGRB rate (Wanderman & Piran 2015) or the cosmic star formation history (Hopkins & Beacom 2006). Each event ejects a fixed amount of r -process material heavier than $A = 90$ with the solar abundance pattern (Goriely 1999; Lodders et al. 2009). The number density of a radioactive nuclide at a given

time t and a point \vec{r} is computed by

$$n_i(t, \vec{r}) = \sum_{j \in t > t_j} \frac{N_i}{K_j(t)} \exp\left(-\frac{|\vec{r} - \vec{r}_j|^2}{4D\Delta t_j} - \frac{\Delta t_j}{\tau_i}\right), \quad (4)$$

where \vec{r}_j and t_j are the location and time of an event labeled by j , $\Delta t_j \equiv t - t_j$, and

$$K_j(t) = \min\left\{(4\pi D\Delta t_j)^{3/2}, 8\pi H D\Delta t_j\right\} \quad (5)$$

where the density evolution changes from the 3-dimensional evolution to the 2-dimensional one appropriately. For ^{244}Pu particles, the total number is given by $N_{\text{Pu}} = ({}^{244}\text{Pu}/{}^{238}\text{U})_0 N_{238\text{U}}$, where $N_{238\text{U}}$ is the number of ^{238}U particles and $({}^{244}\text{P}/{}^{238}\text{U})_0$ is the initial production ratio. This quantity depends on the details of the ejecta properties as well as on the nuclear fission model. In the context of cc-SNe, Cowan et al. (1987) estimated that a ratio of 0.4 reproduces the solar abundance pattern. For compact binary merger ejecta, Eichler et al. (2015) computed a production ratio of 0.33. Here we use $({}^{244}\text{Pu}/{}^{238}\text{U})_0 = 0.4$.

We consider here a characteristic low-rate/high-yield case of $R_0 = 5 \text{ Myr}^{-1}$ following the SGRB rate evolution (Wanderman & Piran 2015) and a high-rate/low-yield case of $R_0 = 300 \text{ Myr}^{-1}$ following the cosmic star formation history (Hopkins & Beacom 2006). Figure 2 shows the results. As expected the fluctuations of the low-rate/high-yield case are much larger than those of the high-rate/low-yield one. For both cases, the estimated range of number densities around 4.6 Gyr BP are consistent with the ESS values and they decrease with time following the decreasing event rate. While for $R_0 = 5 \text{ Myr}^{-1}$ the simulated values are also consistent with the current deep-sea measurements, for $R_0 = 300 \text{ Myr}^{-1}$ the decline is insufficient even when taking the fluctuations into account.

Figure 1 depicts upper and lower bounds on the event rate which consistently explain the ^{244}Pu abundance of the ESS and the current ISM. The sources must satisfy $R_0 \leq 90 \text{ Myr}^{-1}$ and $M_{\text{ej}} \geq 0.001 M_{\odot}$. While these limits vary somewhat with different assumed parameters, the qualitative result that we reach is robust and independent of these choices. We conclude that unless some unknown process suppresses the present amount of ^{244}Pu that reaches Earth, the heavy r -process sources are dominantly low-rate/high-yield ones.

The results should be compared with astronomical observations concerning the possible sources. The low rate clearly rules out cc-SNe. The current ^{244}Pu abundance should be larger by a factor of 5 to 100 to be compatible with a dominant cc-SNe source. Turning to compact binary mergers Fig. 1 depicts also (i) the merger rate estimated from known Galactic binary neutron stars (Kim et al. 2015) and from the current SGRB rate (Wanderman & Piran 2015) and (ii) the ejected mass of r -process elements estimated from macronova candidates associated with GRB 130603B (Tanvir et al. 2013; Berger et al. 2013) and with GRB 060614 Yang et al. (2015) and theoretical ejecta mass estimates (Rosswog 2013; Hotokezaka et al. 2013; Bauswein et al. 2013). Remarkably, the rates and masses estimated here are fully consistent with those observations. In fact most of the overlap between the al-

² The median rather than the average reflects the density that a typical observer measures.

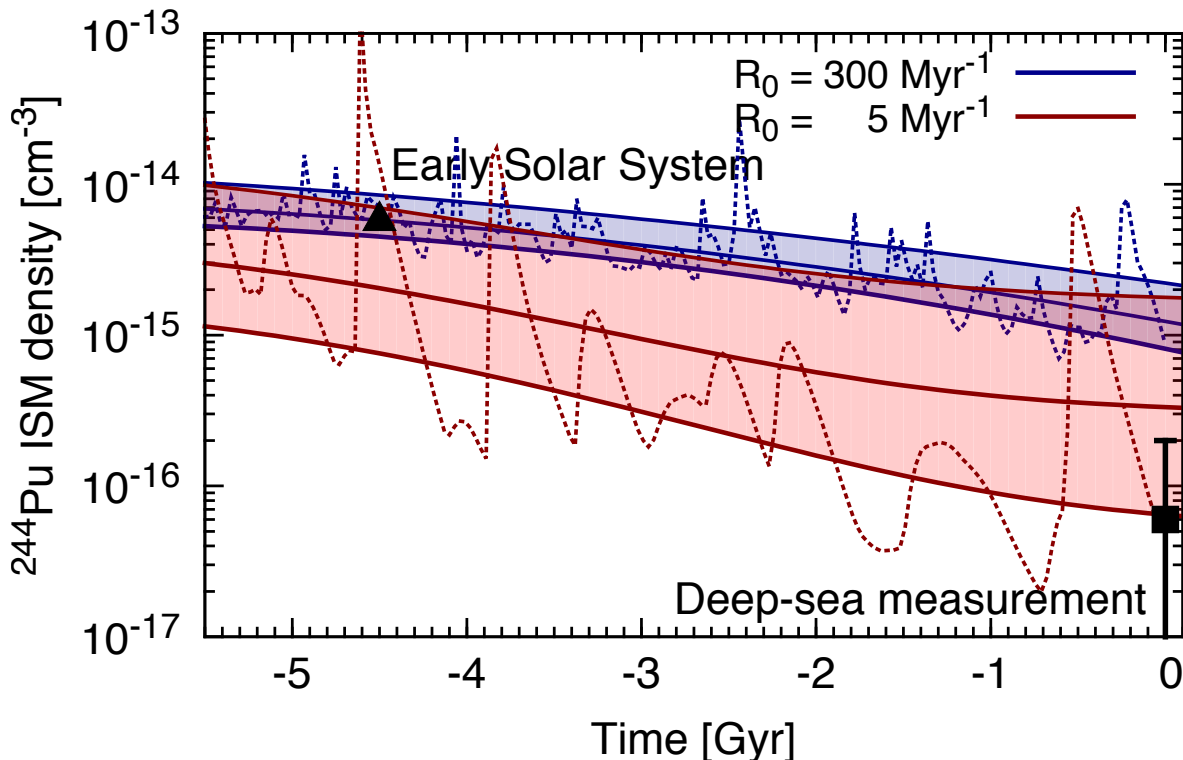


FIG. 2.— Time evolution of ^{244}Pu number densities in the ISM on the solar circle. The solid red (blue) lines represent the median number density and $\pm 1\sigma$ fluctuations for $R_0 = 5 \text{ Myr}^{-1}$ ($R_0 = 300 \text{ Myr}^{-1}$). The lower square with an error bar shows ^{244}Pu density with 2σ limits inferred from the deep sea measurement (Wallner et al. 2015). The triangle at 4.6 Gyr BP shows the value at the time of the ESS (Turner et al. 2007; Lodders et al. 2009). The production rate of ^{244}Pu follows the time evolution of the SGRB rate (Wanderman & Piran 2015) for $R_0 = 5 \text{ Myr}^{-1}$ and the cosmic star formation history (Hopkins & Beacom 2006) for $R_0 = 300 \text{ Myr}^{-1}$. Also shown is an example of the time sequence of ^{244}Pu number densities at a given location on the solar circle from a Monte-Carlo simulation for $R_0 = 5 \text{ Myr}^{-1}$ (dotted red line) and $R_0 = 300 \text{ Myr}^{-1}$ (dotted blue line).

lowed ^{244}Pu region and the overall r -process production range is just in this part of the astrophysical parameter phase space describing compact binary mergers and macronova ejection estimates.

6. SENSITIVITY OF THE RESULTS TO THE CHOICE OF PARAMETERS AND REDSHIFT EVOLUTION

Before proceeding to the conclusion, we show the sensitivity of the results to the choice of parameters. Estimates of the rates and yields involve two unknown parameters: a parameter ϵ and the mixing-length parameter α (see Appendix for details of ϵ). The first, ϵ , introduces the largest uncertainty in the results. For larger values of ϵ , smaller yields are sufficient, as the depletion of the current ISM ^{244}Pu is more significant. Figure 3 shows the rate-yield estimates for $\epsilon = 0.01$ (top panel) and for 0.9 (bottom panel). For $\epsilon = 0.01$, the estimated rate is $R_0 < 7000 \text{ Myr}^{-1}$ within the 2σ level. Even though this rate is quite high it is still smaller than the rate of normal cc-SNe by a factor of a few. For $\epsilon = 0.9$, the allowed event rate is small $R_0 < 7 \text{ Myr}^{-1}$.

The rate-yield estimates with different choices of α (0.3, 0.03, and 0.01) are shown in Fig. 4 and Fig. 5. For $\alpha = 0.3$ (top panel of Fig. 4), the mixing timescale is shorter, implying that a single event can injects live ^{244}Pu particles into a larger volume. As a result, observers measure larger ^{244}Pu densities and the allowed rate-yield region in the figure shifts to the lower event rate compared to those with $\alpha = 0.1$. On the contrary, with a smaller, $\alpha = 0.03$ (bottom panel of Fig. 4) and 0.01 in Fig. 5, higher rates and smaller yields are allowed. Although the overlap region of the ^{244}Pu measurements and total mass of r -process elements depends on the value of ϵ and α , the estimate ranges of the rate and yield are consistent with those of compact binary mergers irrespective of the exact choice of these two parameters. Thus we can generally conclude that the low-rate/high-yield scenario, or more specifically the compact binary merger scenario is preferred while the high-rate/low-yield scenario, or more specifically the cc-SNe scenario, is ruled out.

The time evolution of the mean abundance of ^{244}Pu and its fluctuations depend on the history of the pro-

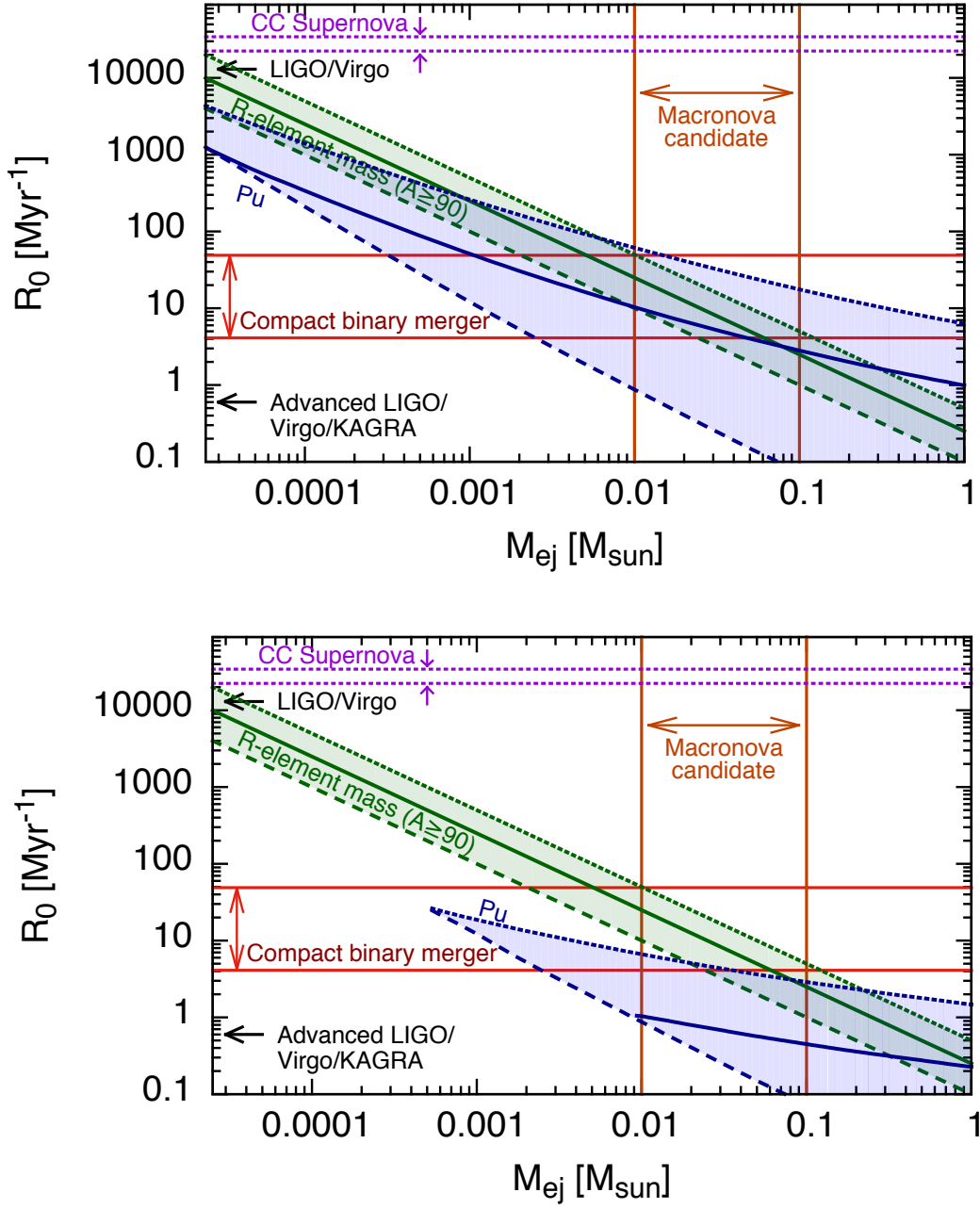


FIG. 3.— Same as Fig. 1 but for the efficiency parameter $\epsilon = 0.01$ (top) and 0.9 (bottom).

duction rate. Figure 6 depicts the rate-yield results with the production rate following the SGRB rate (top panel) and the cosmic star formation history (bottom panel). In both cases, the rate decreases with time for the epoch that we are interested in here. The production rate at 4.6 Gyr BP is higher than the current one by a factor of 3 for the former and 4 for the latter. As long as the event rate decreases by these factors, the results do not depend sensitively on the choice of the production-rate history. However, if the event rate is constant with time, very large fluctuations, i.e., small event rates, are required to be consistent with both the ESS and current measurements as shown in Fig. 7.

7. CONCLUSION AND DISCUSSION

We estimate the expected median value of the ^{244}Pu abundances and fluctuations around this value in the high-rate/low-yield and low-rate/high-yield models and we show that while the current and ESS abundances are naturally explained within the low-rate/high-yield scenario they are incompatible with the high-rate/low-yield (cc-SNe) model. Remarkably, the rates and masses estimated here are fully consistent with astronomical observations of compact binary mergers. In fact most of the overlap between the allowed ^{244}Pu region and the overall r -process production range is just in this part of the

astrophysical parameter phase space describing compact binary mergers and macronova ejection estimates. This result is independent of the choice of the efficiency and diffusion parameters.

Compact binary mergers, which we can conclude are the sources of heavy r -process nucleosynthesis, are also the prime candidates of sources for the upcoming gravitational wave detectors, advanced LIGO/Virgo and KAGRA. Our estimates provide an upper limit to the expected detection rate (assuming a detection horizon distance of 200 Mpc): $R_{\text{GW}} \leq 30 \text{ yr}^{-1}$. The estimated ejected mass in each event is significant and this implies that macronovae (Li & Paczyński 1998; Metzger et al. 2010; Barnes & Kasen 2013; Tanaka & Hotokezaka 2013) and radio flares (Nakar & Piran 2011) associated with the gravitational-wave merger events will be detectable.

Acknowledgements We gratefully acknowledge useful discussions with M. Eichler, K. Kashiyama, H. Kimura, E. Nakar, A. Wallner, and D. Wanderman. This work was supported by the ISF I-Core center for excellence in Astrophysics, by CBSF -ISF grant and by a grant from ISA.

REFERENCES

- Abadie, J., et al. 2012, *Phys. Rev. D*, 85, 082002
 Altobelli, N., Kempf, S., Landgraf, M., Srama, R., Dikarev, V., Krüger, H., Moragas-Klostermeyer, G., & Grün, E. 2003, *Journal of Geophysical Research (Space Physics)*, 108, 8032
 Arnould, M., Goriely, S., & Takahashi, K. 2007, *Phys. Rep.*, 450, 97
 Barnes, J., & Kasen, D. 2013, *ApJ*, 775, 18
 Bauswein, A., Goriely, S., & Janka, H.-T. 2013, *ApJ*, 773, 78
 Berger, E., Fong, W., & Chornock, R. 2013, *ApJ*, 774, L23
 Burbidge, E. M., Burbidge, G. R., Fowler, W. A., & Hoyle, F. 1957, *Reviews of Modern Physics*, 29, 547
 Cioffi, D. F., McKee, C. F., & Bertschinger, E. 1988, *ApJ*, 334, 252
 Cowan, J. J., Thielemann, F.-K., & Truran, J. W. 1987, *ApJ*, 323, 543
 —. 1991, *Phys. Rep.*, 208, 267
 Eichler, D., Livio, M., Piran, T., & Schramm, D. N. 1989, *Nature*, 340, 126
 Eichler, M., et al. 2015, *ApJ*, 808, 30
 Fitoussi, C., et al. 2008, *Physical Review Letters*, 101, 121101
 Freiburghaus, C., Rosswog, S., & Thielemann, F.-K. 1999, *ApJ*, 525, L121
 Frisch, P. C., Redfield, S., & Slavin, J. D. 2011, *ARA&A*, 49, 237
 Frisch, P. C., & Slavin, J. D. 2006, *Astrophysics and Space Sciences Transactions*, 2, 53
 —. 2013, *Earth, Planets, and Space*, 65, 175
 Goriely, S. 1999, *A&A*, 342, 881
 Hopkins, A. M., & Beacom, J. F. 2006, *ApJ*, 651, 142
 Hotokezaka, K., Kiuchi, K., Kyutoku, K., Okawa, H., Sekiguchi, Y.-i., Shibata, M., & Taniguchi, K. 2013, *Phys. Rev. D*, 87, 024001
 Kim, C., Perera, B. B. P., & McLaughlin, M. A. 2015, *MNRAS*, 448, 928
 Knie, K., Korschinek, G., Faestermann, T., Dorfi, E. A., Rugel, G., & Wallner, A. 2004, *Physical Review Letters*, 93, 171103
 Landgraf, M., Krüger, H., Altobelli, N., & Grün, E. 2003, *Journal of Geophysical Research (Space Physics)*, 108, 8030
 Lattimer, J. M., & Schramm, D. N. 1974, *ApJ*, 192, L145
 Li, L.-X., & Paczyński, B. 1998, *ApJ*, 507, L59
 Li, W., Chornock, R., Leaman, J., Filippenko, A. V., Poznanski, D., Wang, X., Ganeshalingam, M., & Mannucci, F. 2011, *MNRAS*, 412, 1473
 Lodders, K., Palme, H., & Gail, H.-P. 2009, *Landolt Börnstein*, 44
 Mann, I. 2010, *ARA&A*, 48, 173
 McMillan, P. J. 2011, *MNRAS*, 414, 2446
 Metzger, B. D., et al. 2010, *MNRAS*, 406, 2650
 Nakar, E., & Piran, T. 2011, *Nature*, 478, 82
 Pan, L., & Scannapieco, E. 2010, *ApJ*, 721, 1765
 Paul, M., et al. 2001, *ApJ*, 558, L133
 Qian, Y.-Z., & Wasserburg, G. J. 2007, *Phys. Rep.*, 442, 237
 Rosswog, S. 2013, *Royal Society of London Philosophical Transactions Series A*, 371, 20272
 Roy, J.-R., & Kunth, D. 1995, *A&A*, 294, 432
 Scalo, J., & Elmegreen, B. G. 2004, *ARA&A*, 42, 275
 Sneden, C., Cowan, J. J., & Gallino, R. 2008, *ARA&A*, 46, 241
 Tanaka, M., & Hotokezaka, K. 2013, *ApJ*, 775, 113
 Tanvir, N. R., Levan, A. J., Fruchter, A. S., Hjorth, J., Hounsell, R. A., Wiersema, K., & Tunnicliffe, R. L. 2013, *Nature*, 500, 547
 Turner, G., Busfield, A., Crowther, S. A., Harrison, M., Mojszsis, S. J., & Gilmour, J. 2007, *Earth and Planetary Science Letters*, 261, 491
 Wallner, A., et al. 2015, *Nature Communications*, 6, 5956
 Wanderman, D., & Piran, T. 2015, *MNRAS*, 448, 3026
 Yang, B., et al. 2015, *Nature Communications*, 6, 7323
 Yang, C.-C., & Krumholz, M. 2012, *ApJ*, 758, 48

APPENDIX

INTERPRETATION OF THE DEEP SEA MEASUREMENT

Wallner et al. (2015) measured the number of live ^{244}Pu particles in deep-sea archives, which consist of two samples, crust and sediment. Using the crust sample the estimated flux of ^{244}Pu particles on the Earth's orbit is $f_{\oplus}^{\text{Pu}} = 250_{-205}^{+590} \text{ cm}^{-2} \text{ Myr}^{-1}$ and it is $3000_{-2850}^{+12000} \text{ cm}^{-2} \text{ Myr}^{-1}$ with the sediment sample. The upper and lower values are 2σ limits. The crust sample spans an accumulation time of 25 Myr and the sediment one spans 1.64 Myr. The two estimates are consistent with each other within the 2σ level. Here, we use only the crust sample since it statistically

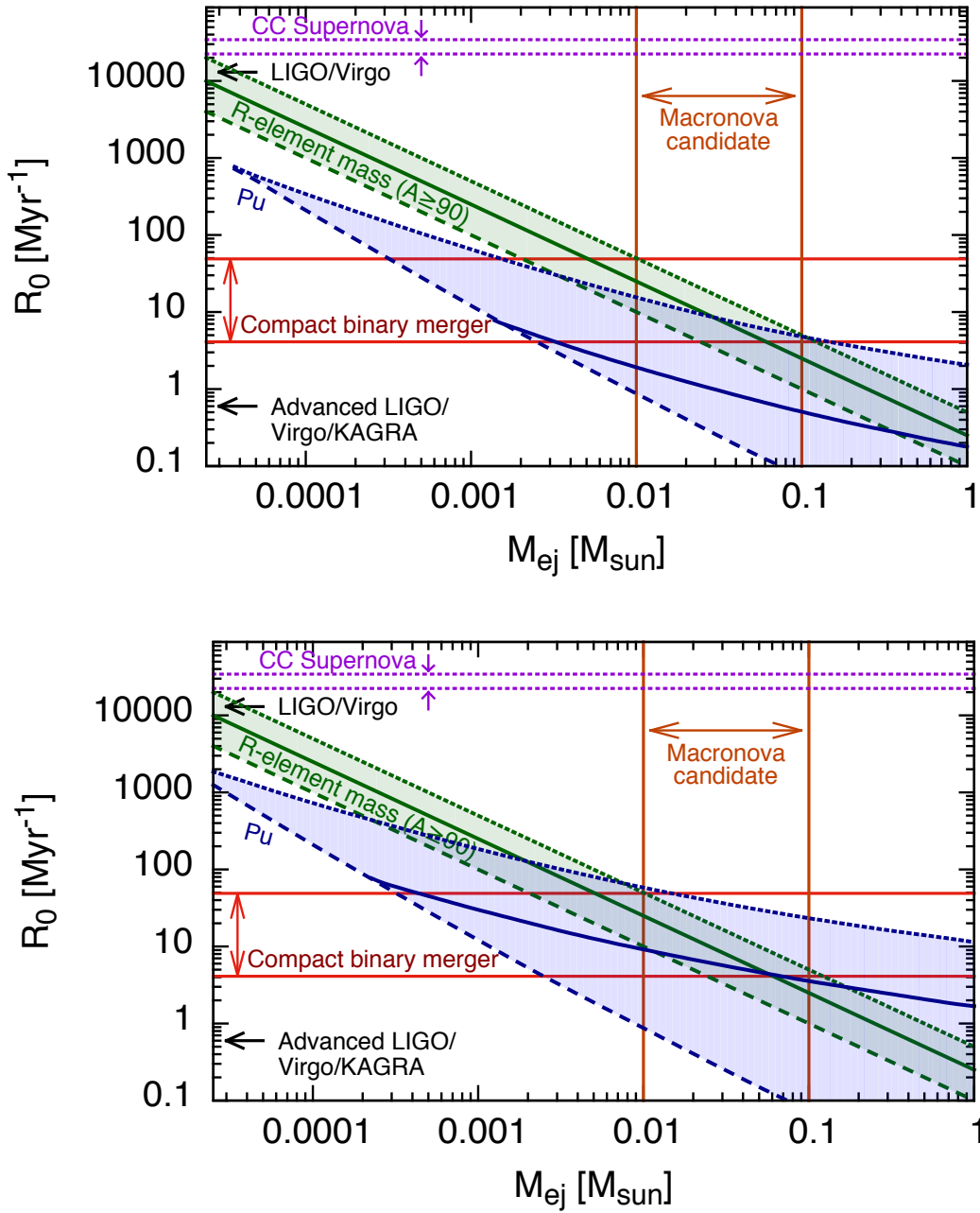


FIG. 4.— Same as Fig. 1 but for the mixing parameter $\alpha = 0.3$ (top) and $\alpha = 0.03$ (bottom).

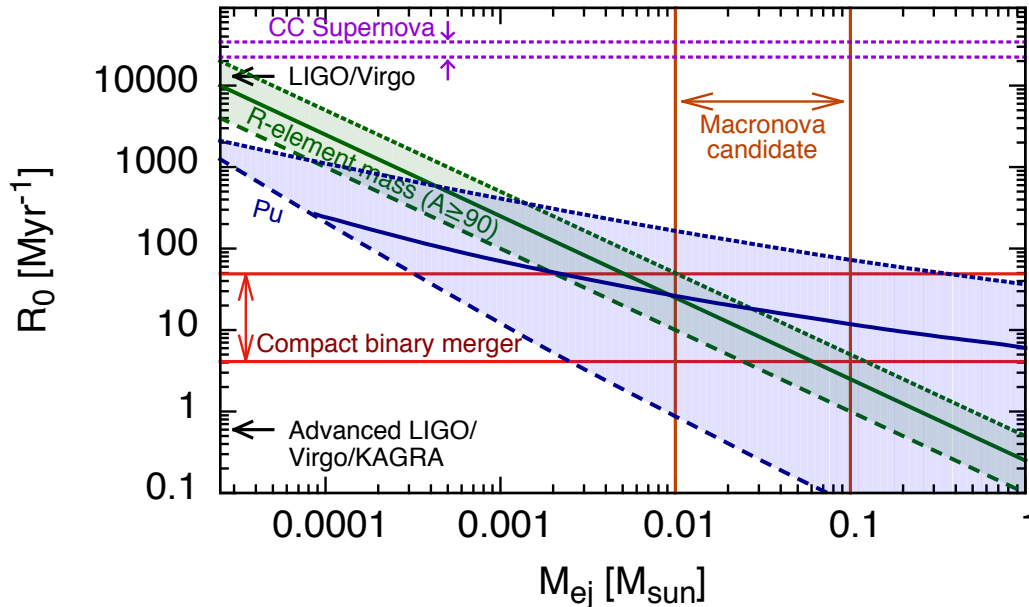


FIG. 5.— Same as Fig. 1 but for the mixing parameter $\alpha = 0.01$.

dominates over the sediment one and it spans a longer accumulation time. Even if one combines the two data, our conclusion does not change significantly. The estimated flux with the two samples combined is $363_{-205}^{+580} \text{ cm}^{-2} \text{ Myr}^{-1}$ where again we take 2σ limits. This is only slightly larger than the one estimated using the crust sample alone.

The value of f_{\oplus}^{Pu} , which is the mean value over the last 25 Myr, is converted to the ^{244}Pu number density in the ISM around the Solar System as

$$n_{\text{ISM}}^{\text{Pu}} = \frac{f_{\oplus}^{\text{Pu}}}{\epsilon v_{\text{rel}}}, \approx 6 \times 10^{-17} \text{ cm}^{-3} \left(\frac{f_{\oplus}^{\text{Pu}}}{250 \text{ cm}^{-2} \text{ Myr}^{-1}} \right) \left(\frac{v_{\text{rel}}}{26 \text{ km/s}} \right)^{-1} (\epsilon)^{-1}, \quad (\text{A1})$$

where v_{rel} is the relative velocity between the Solar System and the ISM. The efficiency ϵ takes into account (i) the penetration efficiency of the ^{244}Pu flux from the ISM outside the heliosphere to the Earth's orbit and (ii) the difference between the mean ISM density around the solar circle and the local ISM density where the Solar System has been traveling during the last 25 Myr. Wallner et al. (2015) used $\epsilon = 0.03\text{--}0.09$. Here we use $\epsilon = 0.05$. In the following, we discuss how this efficiency is estimated.

The dust flux of the ISM inside the heliosphere have been measured by the *Ulysses*, *Galileo*, *Cassini*, and *Helios* spacecrafts (see Mann 2010 for a review). The measurements yield a lower limit on the gas-mass to dust-mass ratio in the local ISM (Frisch & Slavin 2013), ~ 150 , which is roughly consistent with astronomical estimates based on star-light extinction of nearby stars. In addition, the dust flux in a mass range of 5×10^{-14} to 10^{-12} g measured by *Cassini* around 1 AU agrees with the one measured around 3 AU by *Ulysses* during the same period (Landgraf et al. 2003; Altobelli et al. 2003). Based on these facts, we assume that the ^{244}Pu flux on Earth's orbit is the same as the one at the heliopause. We also assume that the ^{244}Pu abundance in the ISM dust grains is independent of the grain size.

As the ISM is highly inhomogeneous, one should take into account the depletion of the local ISM relative to the average galactic ISM density when evaluating the implied radioactive nuclide's density. The Solar System is currently traveling inside a small interstellar cloud (Frisch et al. 2011) with a mean density of $0.1\text{--}0.3 \text{ cm}^{-3}$. This cloud is within the Local Bubble that has a very low mean density of 0.005 cm^{-3} and a radius of $60\text{--}100 \text{ pc}$. Based on the solar motion and the size of the Local Bubble (Frisch & Slavin 2006), the Solar System has been in a very low density region for the last $3\text{--}10 \text{ Myr}$. Before that time it had been outside the Local Bubble, where the ISM density is in the range of $0.1\text{--}1 \text{ cm}^{-3}$. Therefore the ISM density surrounding the Solar System averaged over the last 25 Myr can be estimated as $0.05\text{--}0.9 \text{ cm}^{-3}$.

Based on the above consideration, a plausible range of ϵ is 0.05 to 0.9 . Here we use $\epsilon = 0.05$ as a reference value that corresponds to a conservative choice in terms of the depletion of ^{244}Pu in the ISM. Clearly this is the largest source of uncertainty in our estimates. Still this uncertainty does not affect the qualitative nature of our results. In Sec. 6 we also consider $\epsilon = 0.01$. Even with this low value (see Fig. 3), cc-SNe are only marginally consistent with the deep-sea the measurements. We note also that the penetration of ISM dust to the Earth's orbit in deep-sea archives is confirmed by the observation of a spike of live ^{60}Fe (half-live of 2.6 Myr) in the deep-sea crust (Knie et al. 2004) and sediments (Fitoussi et al. 2008; Wallner et al. in prep). This ^{60}Fe spike is interpreted as direct ejecta of a close-by

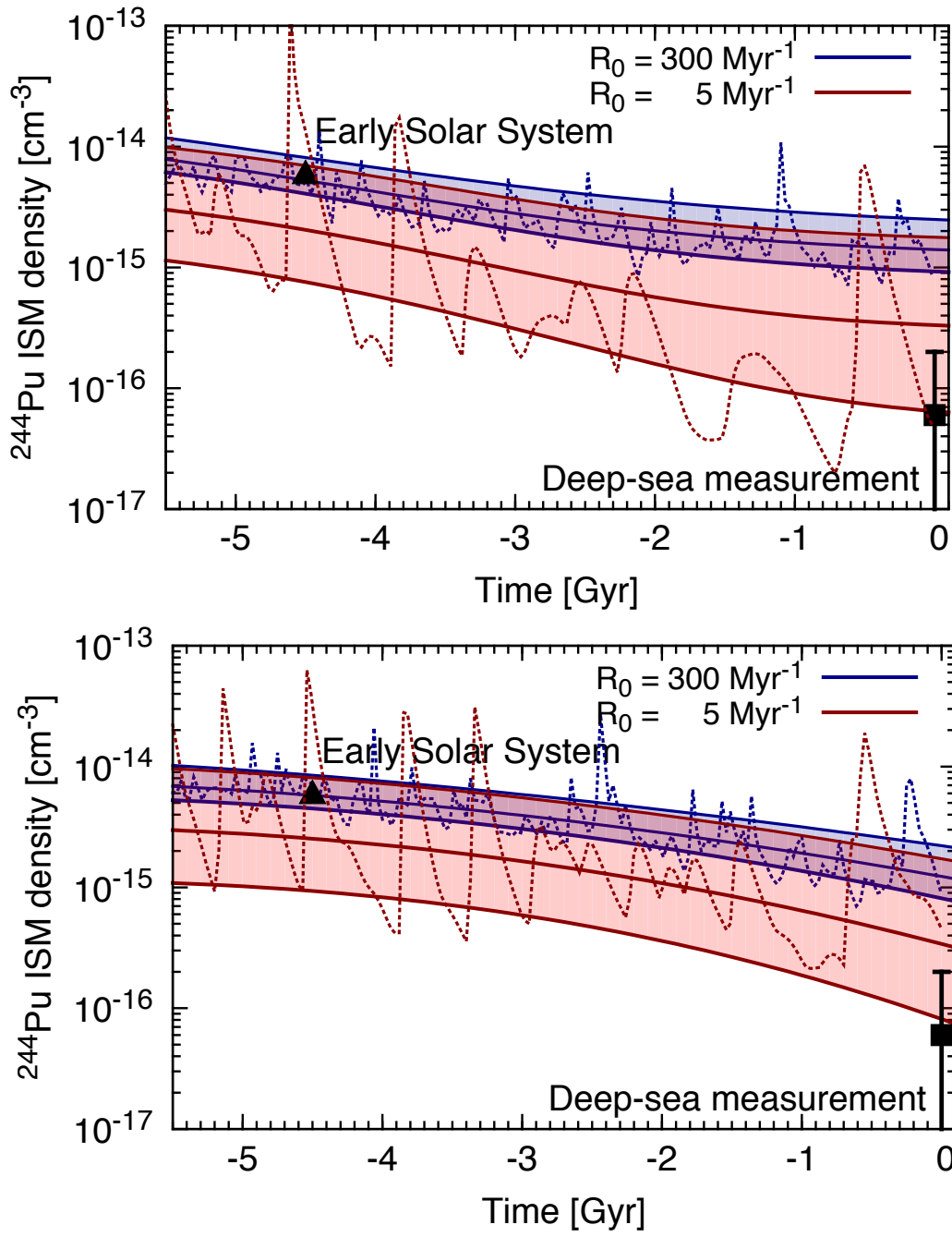


FIG. 6.— Same as Fig. 2 but for the production rate following the SGRB rate (top) and the cosmic star formation history (bottom).

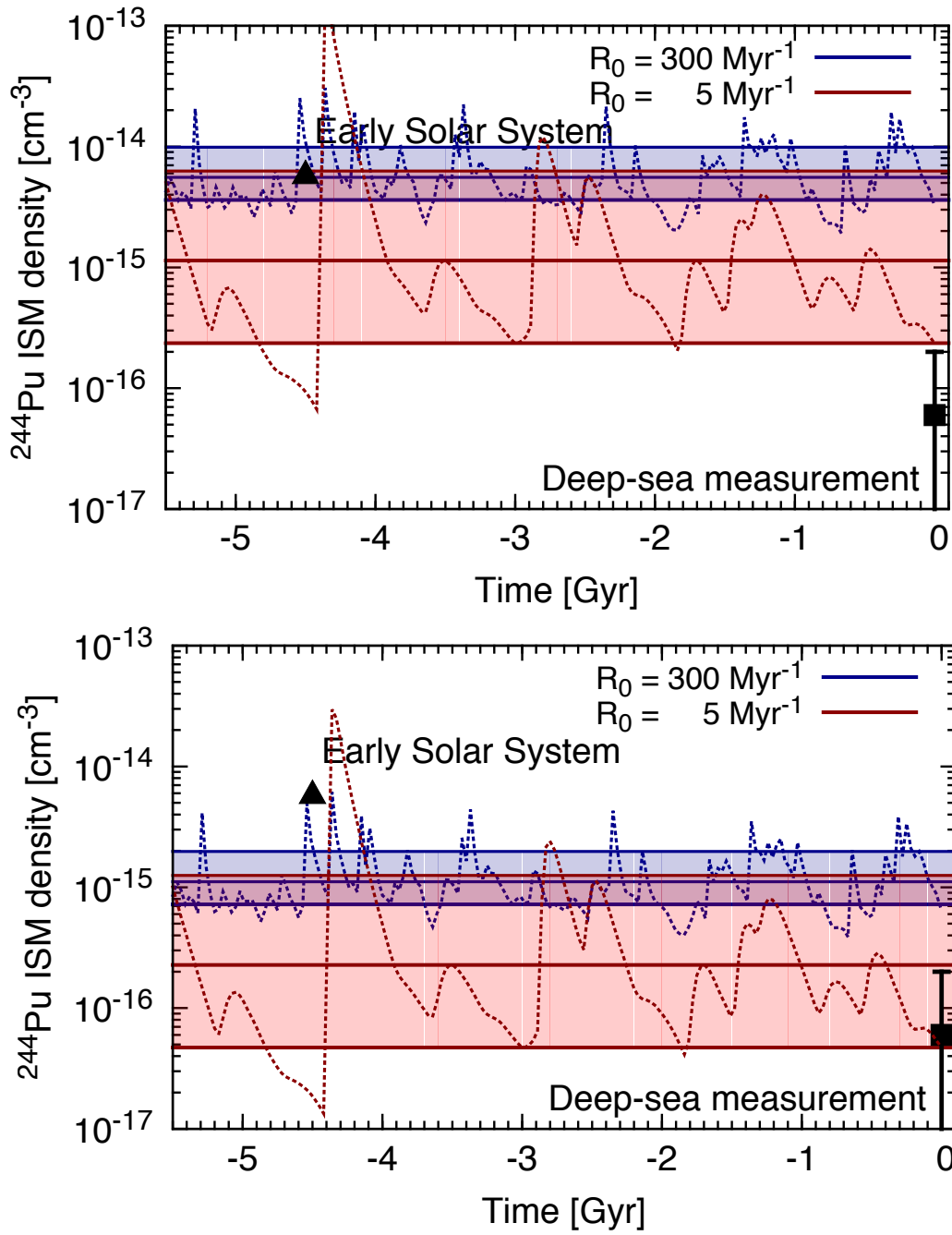


FIG. 7.— Same as Fig. 2 but for a constant production rate. Here we assume $M_{\text{ej}, A \geq 90} = 0.01 M_{\odot} (R/10 \text{ Myr}^{-1})^{-1}$ for the top panel and $M_{\text{ej}, A \geq 90} = 0.05 M_{\odot} (R/10 \text{ Myr}^{-1})^{-1}$ for the bottom panel.

supernova about 2.5 Myr BP.